Self-Trapping of Light and Nonlinear Localized Modes in 2D Photonic Crystals and Waveguides

Serge F. Mingaleev [1,2] and Yuri S. Kivshar [1]

[1] Nonlinear Physics Group, Research School of Physical Sciences and Engineering, The Australian National University, Canberra ACT 0200, Australia
[2] Bogolyubov Institute for Theoretical Physics, Kiev 03143, Ukraine

1 Introduction

Photonic crystals are usually viewed as an optical analog of semiconductors that modify the properties of light similar to a microscopic atomic lattice that creates a semiconductor band-gap for electrons [1]. It is therefore believed that by replacing relatively slow electrons with photons as the carriers of information, the speed and band-width of advanced communication systems will be dramatically increased, thus revolutionizing the telecommunication industry. Recent fabrication of photonic crystals with a band gap at optical wavelengths from 1.35 μm to 1.95 μm makes this promise very realistic [2].

To employ the high-technology potential of photonic crystals, it is crucially important to achieve a dynamical tunability of their band gap [3]. This idea can be realized by changing the light intensity in the so-called *nonlinear photonic crystals*, having a periodic modulation of the nonlinear refractive index [4]. Exploration of *nonlinear properties* of photonic band-gap (PBG) materials is an important direction of research that opens new applications of photonic crystals for all-optical signal processing and switching, allowing an effective way to create tunable band-gap structures operating entirely with light.

One of the important physical concepts associated with nonlinearity is *the energy self-trapping and localization*. In the linear physics, the idea of localization is always associated with disorder that breaks translational invariance. However, during the recent years it was demonstrated that localization can occur in the absence of any disorder and solely due to nonlinearity in the form of *intrinsic localized modes* [5]. A rigorous proof of the existence of time-periodic, spatially localized solutions describing such nonlinear modes has been presented for a broad class of Hamiltonian coupled-oscillator nonlinear lattices [6], but approximate analytical solutions can also be found in many other cases, demonstrating a generality of the concept of *nonlinear localized modes*.

Nonlinear localized modes can be easily identified in numerical molecular-dynamics simulations in many different physical models (see, e.g., Ref. [5] for

a review), but only very recently the *first experimental observations* of spatially localized nonlinear modes have been reported in mixed-valence transition metal complexes [7], quasi-one-dimensional antiferromagnetic chains [8], and arrays of Josephson junctions [9]. Importantly, very similar types of spatially localized nonlinear modes have been experimentally observed in *macroscopic* mechanical [10] and guided-wave optical [11] systems.

Recent experimental observations of nonlinear localized modes, as well as numerous theoretical results, indicate that nonlinearity-induced localization and spatially localized modes can be expected in physical systems of very different nature. From the viewpoint of possible practical applications, self-localized states in optics seem to be the most promising ones; they can lead to different types of nonlinear all-optical switching devices where light manipulates and controls light itself by varying the input intensity. As a result, the study of *nonlinear localized modes in photonic structures* is expected to bring a variety of realistic applications of intrinsic localized modes.

One of the promising fields where the concept of nonlinear localized modes may find practical applications is the physics of *photonic crystals* [or photonic band gap (PBG) materials] – periodic dielectric structures that produce many of the same phenomena for photons as the crystalline atomic potential does for electrons [1]. Three-dimensional (3D) photonic crystals for visible light have been successfully fabricated only within the past year or two, and presently many research groups are working on creating tunable band-gap switches and transistors operating entirely with light. The most recent idea is to employ nonlinear properties of band-gap materials, thus creating *nonlinear photonic crystals* including those where nonlinear susceptibility is periodic as well [4,12].

Nonlinear photonic crystals (or photonic crystals with embedded nonlinear impurities) create an ideal environment for the generation and observation of nonlinear localized photonic modes. In particular, the existence of such modes for the frequencies in the photonic band gaps has been predicted [13] for 2D and 3D photonic crystals with Kerr nonlinearity. Nonlinear localized modes can be also excited at nonlinear interfaces with quadratic nonlinearity [14], or along dielectric waveguide structures possessing a nonlinear Kerr-type response [15].

In this Chapter, we study self-trapping of light and nonlinear localized modes in nonlinear photonic crystals and photonic crystal waveguides. For simplicity, we consider the case of a 2D photonic crystal with embedded nonlinear rods (impurities) and demonstrate that the effective interaction in such a structure is nonlocal, so that the nonlinear effects can be described by a nontrivial generalization of the nonlinear lattice models that include the long-range coupling and nonlocal nonlinearity. We describe several different types of nonlinear guided-wave states in photonic crystal waveguides and analyse their properties [16]. Also, we predict the existence of *stable* nonlinear

localized modes (highly localized modes analogous to gap solitons in the continuum limit) in the reduced-symmetry nonlinear photonic crystals [17].

2 Basic Equations

Let us consider a 2D photonic crystal created by a periodic lattice of parallel, infinitely long dielectric rods in air (see Fig. 1). We assume that the rods are parallel to the x_3 axis, so that the system is characterized by the dielectric constant $\varepsilon(\boldsymbol{x}) = \varepsilon(x_1, x_2)$. As is well known [1], the photonic crystals of this type can possess a complete band gap for the E-polarized (with the electric field $\boldsymbol{E} \,||\, \boldsymbol{x}_3$) light propagating in the (x_1, x_2)-plane. The evolution of such a light is governed by the scalar wave equation

$$\nabla^2 E(\boldsymbol{x}, t) - \frac{1}{c^2}\,\partial_t^2\,[\varepsilon(\boldsymbol{x}) E] = 0\;, \tag{1}$$

where $\nabla^2 \equiv \partial_{x_1}^2 + \partial_{x_2}^2$ and E is the x_3 component of $\boldsymbol{E}$. Taking the electric field in the form $E(\boldsymbol{x}, t) = \mathrm{e}^{-\mathrm{i}\omega t}\, E(\boldsymbol{x}, t\,|\,\omega)$, where $E(\boldsymbol{x}, t\,|\,\omega)$ is a slowly varying envelope, i.e. $\partial_t^2 E(\boldsymbol{x}, t\,|\,\omega) \ll \omega \partial_t E(\boldsymbol{x}, t\,|\,\omega)$, Eq. (1) reduces to

$$\left[\nabla^2 + \varepsilon(\boldsymbol{x}) \left(\frac{\omega}{c}\right)^2\right] E(\boldsymbol{x}, t\,|\,\omega) \simeq -2\,\mathrm{i}\,\varepsilon(\boldsymbol{x}) \frac{\omega}{c^2}\,\frac{\partial E}{\partial t}\;. \tag{2}$$

In the stationary case, i.e. when the r.h.s. of Eq. (2) vanishes, this equation describes an eigenvalue problem which can be solved, e.g. by the plane waves method [18], in the case of a perfect photonic crystal, for which the dielectric constant $\varepsilon(\boldsymbol{x}) \equiv \varepsilon_p(\boldsymbol{x})$ is a periodic function defined as

$$\varepsilon_p(\boldsymbol{x} + \boldsymbol{s}_{ij}) = \varepsilon_p(\boldsymbol{x})\;, \tag{3}$$

where i and j are arbitrary integers, and

$$\boldsymbol{s}_{ij} = i\,\boldsymbol{a}_1 + j\,\boldsymbol{a}_2 \tag{4}$$

is a linear combination of the lattice vectors $\boldsymbol{a}_1$ and $\boldsymbol{a}_2$.

For definiteness, we consider the 2D photonic crystal earlier analyses (in the linear limit) in Refs. [19,20]. That is, we assume that cylindrical rods with radius $r_0 = 0.18a$ and dielectric constant $\varepsilon_0 = 11.56$ form a square lattice with the distance a between two neighboring rods, so that $\boldsymbol{a}_1 = a\boldsymbol{x}_1$ and $\boldsymbol{a}_2 = a\boldsymbol{x}_2$. The frequency band structure for this type of 2D photonic crystal is shown in Fig. 1 where, using the notations of the solid-state physics, the wave dispersion is mapped onto the Brillouin zone of the so-called *reciprocal lattice* that faces are known as Γ, M, and X. As follows from Fig. 1, there exists a large (38%) band gap that extends from the lower cut-off frequency, $\omega = 0.302 \times 2\pi c/a$, to the upper band-gap frequency, $\omega = 0.443 \times 2\pi c/a$. If the frequency of a low-intensity light falls into the band gap, the light cannot propagate through the photonic crystal and is reflected.

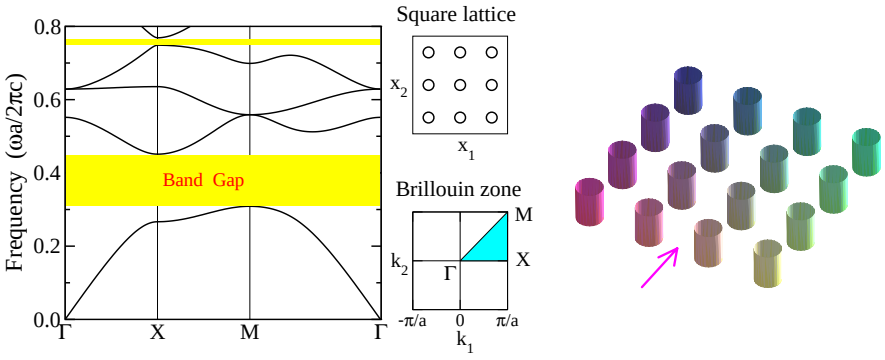

Fig. 1. The band-gap structure of the photonic crystal consisting of a square lattice of dielectric rods with $r_0 = 0.18a$ and $\varepsilon_0 = 11.56$ (the band gaps are shaded). The top center inset shows a cross-sectional view of the 2D photonic crystal depicted in the right inset. The bottom center inset shows the corresponding Brillouin zone, with the irreducible zone shaded.

3 Defect Modes: The Green Function Approach

One of the most intriguing properties of photonic band gap crystals is the emergence of exponentially localized modes that may appear within the photonic band gaps when a defect is embedded into an otherwise perfect photonic crystal. The simplest way to create a defect in a 2D photonic crystal is to introduce an additional defect rod with the radius r_d and the dielectric constant $\varepsilon_d(\boldsymbol{x})$. In this case, the dielectric constant $\varepsilon(\boldsymbol{x})$ can be presented as a sum of periodic and defect-induced terms, i.e.

$$\varepsilon(\boldsymbol{x}) = \varepsilon_p(\boldsymbol{x}) + \varepsilon_d(\boldsymbol{x}) \,,$$

and, therefore, Eq. (2) takes the form

$$\left[\nabla^2 + \left(\frac{\omega}{c}\right)^2 \varepsilon_p(\boldsymbol{x})\right] E(\boldsymbol{x}, t \,|\, \omega) = -\hat{\mathcal{L}} E(\boldsymbol{x}, t \,|\, \omega) \,, \tag{5}$$

where the operator

$$\hat{\mathcal{L}} = \left(\frac{\omega}{c}\right)^2 \varepsilon_d(\boldsymbol{x}) + 2\,\mathrm{i}\,\varepsilon(\boldsymbol{x}) \frac{\omega}{c^2} \frac{\partial}{\partial t} \tag{6}$$

is introduced for convenience. Equation (5) can also be written in the equivalent integral form

$$E(\boldsymbol{x}, t \,|\, \omega) = \int \mathrm{d}^2\boldsymbol{y}\;\; G(\boldsymbol{x}, \boldsymbol{y} \,|\, \omega)\, \hat{\mathcal{L}}\, E(\boldsymbol{y}, t \,|\, \omega) \,, \tag{7}$$

where $G(\boldsymbol{x}, \boldsymbol{y} \,|\, \omega)$ is the Green function defined, in a standard way, as a solution of the equation

$$\left[\nabla^2 + \left(\frac{\omega}{c}\right)^2 \varepsilon_p(\boldsymbol{x})\right] G(\boldsymbol{x}, \boldsymbol{y} \,|\, \omega) = -\delta(\boldsymbol{x} - \boldsymbol{y}) \,. \tag{8}$$

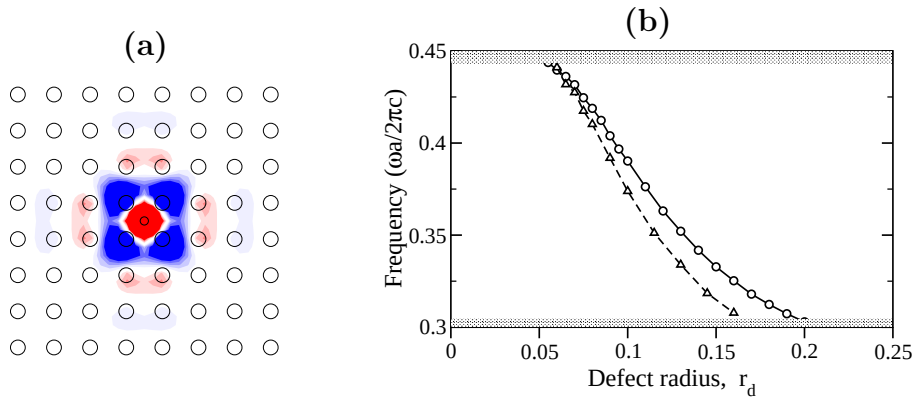

Fig. 2. (a) Electric field structure of a linear localized mode supported by a single defect rod with radius $r_d = 0.1a$ and $\varepsilon_d = 11.56$ in a square-lattice photonic crystal with $r_0 = 0.18a$ and $\varepsilon_0 = 11.56$. The rod positions are indicated by circles and the amplitude of the electric field is indicated by color. **(b)** Frequency of the defect mode as a function of the radius r_d: calculated precisely from Eq. (7) (*full line with circles*) and approximately from Eq. (15) (*dashed line with triangles*).

General properties of the Green function of a perfect 2D photonic crystal are described in more details in Ref. [18]. Here, we notice that the Green function is *symmetric*, i.e.

$$G(\boldsymbol{x}, \boldsymbol{y} \,|\, \omega) = G(\boldsymbol{y}, \boldsymbol{x} \,|\, \omega)$$

and *periodic*, i.e.

$$G(\boldsymbol{x} + \boldsymbol{s}_{ij}, \boldsymbol{y} + \boldsymbol{s}_{ij} \,|\, \omega) = G(\boldsymbol{x}, \boldsymbol{y} \,|\, \omega) \ ,$$

where $\boldsymbol{s}_{ij}$ is defined by Eq. (4).

The Green function can be calculated by means of the Fourier transform

$$G(\boldsymbol{x}, \boldsymbol{y} \,|\, \omega) = \int_{-\infty}^{\infty} \mathrm{d}t \ \ e^{\mathrm{i}\omega t} G(\boldsymbol{x}, \boldsymbol{y}, t) \tag{9}$$

applied to the time-dependent Green function governed by the equation

$$\left[\nabla^2 - \varepsilon_p(\boldsymbol{x})\, \partial_t^2\right] G(\boldsymbol{x}, \boldsymbol{y}, t) = -\delta(t)\, \delta(\boldsymbol{x} - \boldsymbol{y}) \ , \tag{10}$$

which has been solved by the finite-difference time-domain method [21].

Now that we have calculated the Green function, we can figure out the defect states solving Eq. (7) directly. For example, Fig. 2(a) shows a defect mode created by introducing a single defect rod with the radius $r_d = 0.1a$ and dielectric constant $\varepsilon_d = 11.56$ into the 2D photonic crystal shown in Fig. 1. Although direct numerical solution of the integral equation (7) remains possible even in the case of a few defect rods, it becomes severely limited by

the current computer facilities as soon as we increase the number of the defect rods and start investigation of the line defects (waveguides) and their branches. Thus, looking for new approximate numerical techniques which could combine reasonable accuracy, flexibility, and power to forecast new effects is an issue of the key importance.

4 Effective discrete equations

Studying the electric field distribution of the defect mode in Fig. 2(a), one can suggest that a reasonably accurate approximation should be provided by the assumption that the electric field inside the defect rod remains constant. Indeed, let us assume that nonlinear defect rods embedded into a photonic crystal are located at the points $\boldsymbol{x}_m$, where m is the index (or a combination of two indices in the case of a two-dimensional array of defect rods) introduced for explicit numbering of the defect rods. In this case, the correction to the dielectric constant is

$$\varepsilon_d(\boldsymbol{x}) = \left\{ \varepsilon_d^{(0)} + |E(\boldsymbol{x}, t \,|\, \omega)|^2 \right\} \sum_m \theta(\boldsymbol{x} - \boldsymbol{x}_m) \;, \tag{11}$$

where

$$\theta(\boldsymbol{x}) = \begin{cases} 1 \;, & \text{for} \quad |\boldsymbol{x}| \le r_d \;, \\ 0 \;, & \text{for} \quad |\boldsymbol{x}| > r_d \;. \end{cases} \tag{12}$$

The second term in Eq. (11) takes into account a contribution due to the Kerr nonlinearity (we assume that the electric field is scaled with the nonlinear susceptibility, $\chi^{(3)}$). Assuming, as we discussed above, that the electric field $E(\boldsymbol{x}, t \,|\, \omega)$ inside the defect rods is almost constant, one can derive, by substituting Eq. (11) into Eq. (7) and averaging over the cross-section of the rods [15], an approximate *discrete nonlinear equation*

$$i\sigma \frac{\partial}{\partial t} E_n - E_n + \sum_m J_{n-m}(\omega)(\varepsilon_d^{(0)} + |E_m|^2) E_m = 0 \;, \tag{13}$$

for the amplitudes of the electric field $E_n(t \,|\, \omega) \equiv E(\boldsymbol{x}_n, t \,|\, \omega)$ inside the defect rods. The parameter σ and the coupling constants

$$J_n(\omega) = \left(\frac{\omega}{c}\right)^2 \int_{r_d} d^2\boldsymbol{y} \;\; G(\boldsymbol{x}_0, \boldsymbol{x}_n + \boldsymbol{y} \,|\, \omega) \tag{14}$$

are determined in this case by the Green function $G(\boldsymbol{x}, \boldsymbol{y} \,|\, \omega)$ of the perfect photonic crystal.

To check the accuracy of the approximation provided by Eq. (13), we solved it in the linear limit for the case of a single defect rod. In this case Eq. (13) is reduced to the equation

$$J_0(\omega_d) = 1/\varepsilon_d^{(0)} \;, \tag{15}$$

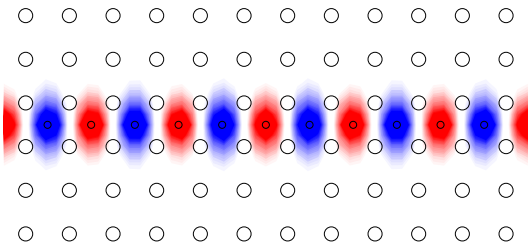

Fig. 3. Electric field of the linear guiding mode in a waveguide created by an array of the defect rods. The rod positions are indicated by circles and the amplitude of the electric field is indicated by color.

from which one can obtain an estimation for the frequency ω_d of the localized defect mode. As is seen from Fig. 2(b), the mode frequency calculated in the framework of this approximation is in a good agreement with that calculated directly from Eq. (7), provided the defect radius r_d is small enough. Even for $r_d = 0.15a$ an error introduced by the approximation does not exceed 5%. It lends a support to the validity of Eq. (13) allowing us to use it hereafter for studying nonlinear localized modes.

5 Nonlinear Waveguides in 2D Photonic Crystals

One of the most promising applications of the PBG structures is a possibility to create a novel type of optical waveguides. In conventional waveguides such as optical fibers, light is confined by *total internal reflection* due a difference in the refractive indices of the waveguide core and cladding. One of the weaknesses of such waveguides is that creating of bends is difficult. Unless the radius of the bend is large compared to the wavelength, much of the light will be lost. This is a serious obstacle for creating "integrated optical circuits", since the space required for large-radius bends is unavailable.

The waveguides based on the PBG materials employ *a different physical mechanism*: the light is guided by a line of coupled defects which possess a localized defect mode with frequency inside the band gap. The simplest photonic-crystal waveguide can be created by a straight line of defect rods, as shown in Fig. 3. Instead of a single localized state of an isolated defect, a waveguide supports propagating states (guided modes) with the frequencies in a narrow band located inside the band gap of a perfect crystal. Such guided modes have a periodical profile along the waveguide, and they decay exponentially in the transverse direction, see Fig. 3. That is, photonic crystal waveguides operate in a manner similar to resonant cavities, and the light with guiding frequencies is forbidden from propagating in the bulk. Because of this, when a bend is created in a photonic crystal waveguide, the light remains trapped and the only possible problem is that of reflection. However,

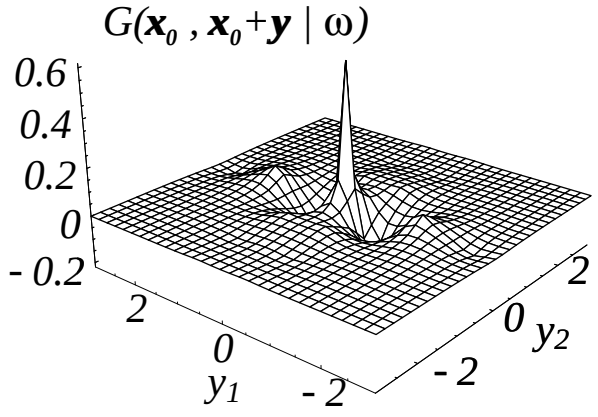

Fig. 4. The Green function $G(\boldsymbol{x}_0, \boldsymbol{x}_0+\boldsymbol{y}\,|\,\omega)$ for the photonic crystal shown in Fig. 1 ($\boldsymbol{x}_0 = \boldsymbol{a}_1/2$ and $\omega = 0.33 \times 2\pi c/a$).

as was predicted numerically [19,20] and then demonstrated in microwave [22] and optical [23] experiments, it is still possible to get very high transmission efficiency for nearly all frequencies inside the gap.

To employ the high-technology potential of photonic crystal waveguides, it is crucially important to achieve a tunability of their transmission properties. Nowadays, several approaches have been suggested for this purpose. For instance, it has been recently demonstrated both numerically [24] and in microwave experiments [25], that transmission spectrum of straight and sharply bent waveguides in *quasiperiodic photonic crystals* is rather rich in structure and only some frequencies get near perfect transmission. Another possibility is creation of the *channel drop system* on the bases of two parallel waveguides coupled by the point defects between them. It has been shown [26] that high-Q frequency selective complete transfer can occur between such waveguides by creating resonant defect states of different symmetry and by forcing an accidental degeneracy between them.

However, being frequency selective, the above mentioned approaches do not possess *dynamical tunability* of the transmission properties. The latter idea can be realized by changing the light intensity in the so-called *nonlinear photonic crystal waveguides* [16], created by inserting an additional row of rods made from a Kerr-type nonlinear material characterized by the third-order nonlinear susceptibility $\chi^{(3)}$ and the linear dielectric constant $\varepsilon_d^{(0)}$. For definiteness, we assume that $\varepsilon_d^{(0)} = \varepsilon_0 = 11.56$ and that the nonlinear defect rods are embedded into the photonic crystal along a selected direction $\boldsymbol{s}_{ij}$, so that they are located at the points $\boldsymbol{x}_m = \boldsymbol{x}_0 + m\,\boldsymbol{s}_{ij}$. As we show below, changing the radius r_d of these defect rods and their location $\boldsymbol{x}_0$ in the crystal, one can create nonlinear waveguides with quite different properties.

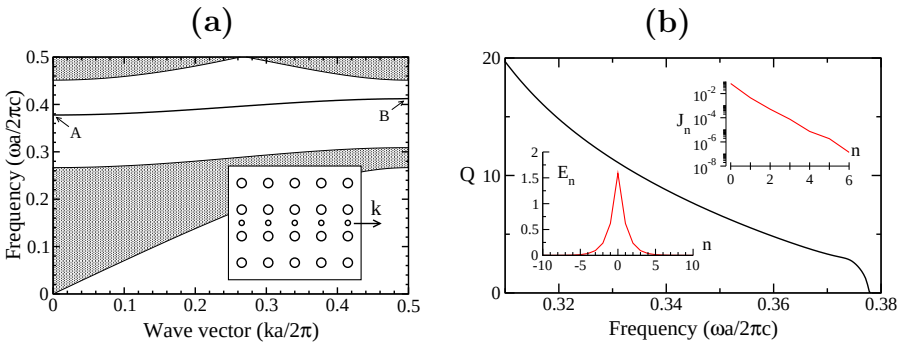

Fig. 5. **(a)** Dispersion relation for the photonic crystal waveguide shown in the inset ($\varepsilon_0 = \varepsilon_d = 11.56$, $r_0 = 0.18a$, $r_d = 0.10a$). The grey areas are the projected band structure of the perfect 2D photonic crystal. The frequencies at the indicated points are: $\omega_A = 0.378 \times 2\pi c/a$ and $\omega_B = 0.412 \times 2\pi c/a$. **(b)** Mode power $Q(\omega)$ of the nonlinear mode excited in the corresponding photonic crystal waveguide. The right inset gives the dependence $J_n(\omega)$ calculated at $\omega = 0.37 \times 2\pi c/a$. The left inset presents the profile of the corresponding nonlinear localized mode.

As we have already discussed [16,17], the Green function $G(\boldsymbol{x}, \boldsymbol{y} \,|\, \omega)$ and, consequently, the coupling coefficients $J_m(\omega)$ are usually highly long-ranged functions. This can be seen directly from Fig. 4 that shows a typical spatial profile of the Green function. As a consequence, the coupling coefficients $J_n(\omega)$ calculated from Eq. (14) decrease slowly with the site number n. For $\boldsymbol{s}_{01}$ and $\boldsymbol{s}_{10}$ directions, the coupling coefficients can be approximated by an exponential function as follows

$$|J_n(\omega)| \approx \begin{cases} J_0(\omega)\,, & \text{for } \; n = 0\,, \\ J_*(\omega)\, e^{-\alpha(\omega)|n|}\,, & \text{for } |n| \geq 1\,, \end{cases}$$

where the characteristic decay rate $\alpha(\omega)$ can be as small as 0.85, depending on the values of ω, $\boldsymbol{x}_0$, and r_d, and it can be even smaller for other types of photonic crystals (for instance, for the photonic crystal used in Fig. 12 we find $J_m \sim (-1)^m \exp(-0.66m)$ for $m \geq 2$). By this means, Eq. (13) is a non-trivial long-range generalization of a 2D discrete nonlinear Schrödinger (NLS) equation extensively studied during the last decade for different applications [34]. It allows us to draw an analogy between the problem under consideration and a class of the NLS equations that describe nonlinear excitations in quasi-one-dimensional molecular chains with long-range (e.g. dipole-dipole) interaction between the particles and local on-site nonlinearities [27,28]. For such systems, it was shown that the effect of nonlocal interparticle interaction brings some new features to the properties of nonlinear localized modes (in particular, bistability in their spectrum). Moreover, for our model the coupling coefficients $J_n(\omega)$ can be either unstaggered and monotonically decaying, i.e. $J_n(\omega) = |J_n(\omega)|$, or staggered and oscillating from site to site,

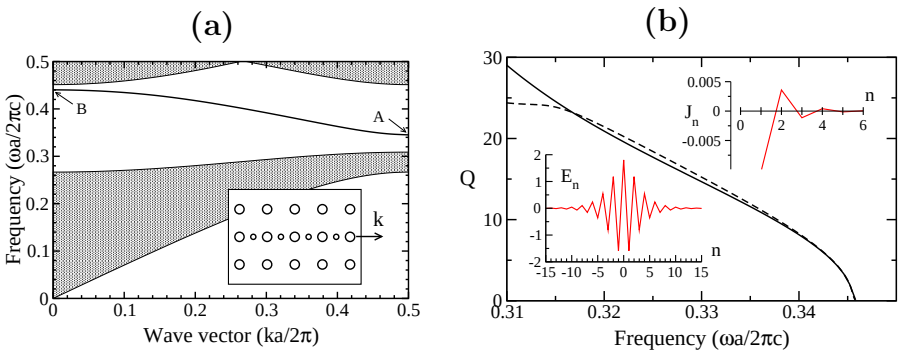

Fig. 6. **(a)** Dispersion relation for the photonic crystal waveguide shown in the inset ($\varepsilon_0 = \varepsilon_d = 11.56$, $r_0 = 0.18a$, $r_d = 0.10a$). The grey areas are the projected band structure of the perfect 2D photonic crystal. The frequencies at the indicated points are: $\omega_A = 0.346 \times 2\pi c/a$ and $\omega_B = 0.440 \times 2\pi c/a$. **(b)** Mode power $Q(\omega)$ of the nonlinear mode excited in the corresponding photonic crystal waveguide. Two cases are presented: the case of nonlinear rods in a linear photonic crystal (*solid line*) and the case of a completely nonlinear photonic crystal (*dashed line*). The right inset shows the behavior of the coupling coefficients $J_n(\omega)$ for $n \geq 1$ ($J_0 = 0.045$) at $\omega = 0.33 \times 2\pi c/a$. The left inset shows the profile of the nonlinear mode.

i.e. $J_n(\omega) = (-1)^n |J_n(\omega)|$. We therefore expect that effective nonlocality in both linear and nonlinear terms of Eq. (13) may also bring similar new features into the properties of nonlinear localized modes excited in the photonic crystal waveguides.

5.1 Staggered and unstaggered localized modes

As can be seen from the structure of the Green function presented in Fig. 4, the case of monotonically varying coefficients $J_n(\omega)$ can occur for the waveguide oriented in the $\boldsymbol{s}_{01}$ direction with $\boldsymbol{x}_0 = \boldsymbol{a}_1/2$. In this case, the frequency of a linear guided mode, that can be excited in such a waveguide, takes a minimum value at $k = 0$ [see Fig. 5(a)], and the corresponding nonlinear mode is expected to be unstaggered.

We have solved Eq. (13) numerically and found that nonlinearity can lead to the existence of *guided modes localized in both directions*, i.e. in the direction perpendicular to the waveguide, due to the guiding properties of a channel waveguide created by defect rods, and in the direction of the waveguide, due to the nonlinearity-induced self-trapping effect. Such nonlinear modes exist with the frequencies below the frequency of the linear guided mode of the waveguide, i.e. below the frequency ω_A in Fig. 5(a), and are indeed unstaggered, with the bell-shaped profile along the waveguide direction shown in the left inset of Fig. 5(b).

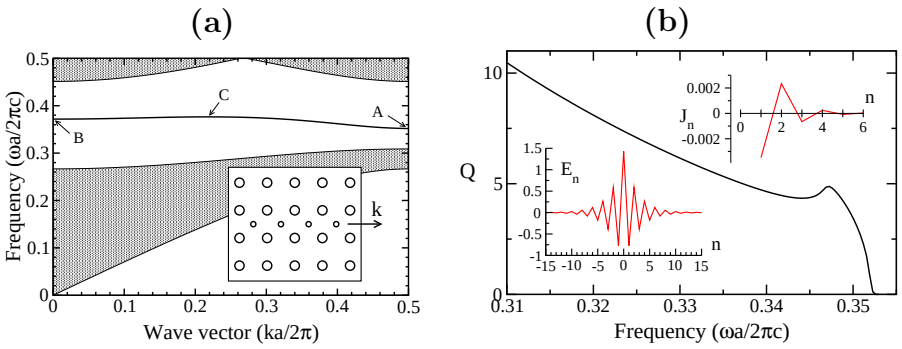

Fig. 7. **(a)** Dispersion relation for the photonic crystal waveguide shown in the inset ($\varepsilon_0 = \varepsilon_d = 11.56$, $r_0 = 0.18a$, $r_d = 0.10a$). The grey areas are the projected band structure of the perfect 2D photonic crystal. The frequencies at the indicated points are: $\omega_A = 0.352 \times 2\pi c/a$, $\omega_B = 0.371 \times 2\pi c/a$, and $\omega_C = 0.376 \times 2\pi c/a$ (at $k = 0.217 \times 2\pi/a$). **(b)** Mode power $Q(\omega)$ of the nonlinear mode excited in the corresponding photonic crystal waveguide. The right inset shows the behavior of the coupling coefficients $J_n(\omega)$ for $n \geq 1$ ($J_0 = 0.068$) at $\omega = 0.345 \times 2\pi c/a$. The left inset shows the profile of the corresponding nonlinear mode.

The 2D nonlinear modes localized in both dimensions can be characterized by the mode power which we define, by analogy with the NLS equation, as

$$Q = \sum_n |E_n|^2. \tag{16}$$

This power is closely related to the energy of the electric field in the 2D photonic crystal accumulated in the nonlinear mode. In Fig. 5(b) we plot the dependence of Q on frequency, for the waveguide geometry shown in Fig. 5(a).

As can be seen from the Green function shown in Fig. 4, the case of staggered coupling coefficients $J_n(\omega)$ can be obtained for the waveguide oriented in the $\boldsymbol{s}_{10}$ direction with $\boldsymbol{x}_0 = \boldsymbol{a}_1/2$. In this case, the frequency dependence of the linear guided mode of the waveguide takes the minimum at $k = \pi/a$ [see Fig. 6(a)]. Accordingly, the nonlinear guided mode localized along the direction of the waveguide is expected to exist with the frequency below the lowest frequency ω_A of the linear guided mode, with a staggered profile. The longitudinal profile of such a 2D nonlinear localized mode is shown in the left inset in Fig. 6(b), together with the dependence of the mode power Q on the frequency (solid curve), which in this case is again monotonic.

The results presented above are obtained for linear photonic crystals with nonlinear waveguides created by a row of defect rods. However, we have carried out the same analysis for the general case of *a nonlinear photonic crystal* that is created by rods of different size but made of the same nonlinear material. Importantly, we have found relatively small difference in all the

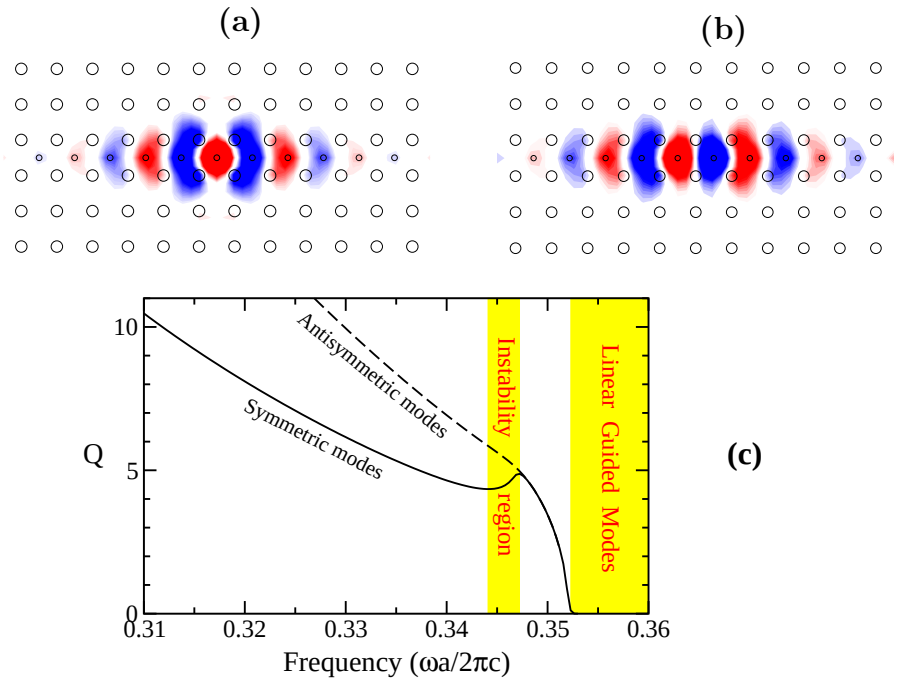

Fig. 8. Examples of the **(a)** symmetric and **(b)** antisymmetric localized modes. The rod positions are indicated by circles and the amplitude of the electric field is indicated by color [red, for positive values, and blue, for negative values]; **(c)** Power Q vs. frequency dependencies calculated for two modes of different symmetry in the photonic crystal waveguide shown in Fig. 7.

results presented above provided nonlinearity is weak. In particular, for the photonic crystal waveguide shown in Fig. 6(a), the results for linear and nonlinear photonic crystals are very close. Indeed, for the mode power Q the results corresponding to a nonlinear photonic crystal are shown in Fig. 6(b) by a dashed curve, and for $Q < 20$ this curve almost coincides with the solid curve corresponding to the case of a nonlinear waveguide embedded into a 2D linear photonic crystal.

5.2 Instability of nonlinear localized modes

Let us now consider the waveguide created by a row of defect rods which are located at the points $\boldsymbol{x}_0 = (\boldsymbol{a}_1 + \boldsymbol{a}_2)/2$, along a straight line in either the $\boldsymbol{s}_{10}$ or $\boldsymbol{s}_{01}$ directions. The results for this case are presented in Figs. 7–8. The coupling coefficients J_n are described by a slowly decaying staggered function of the site number n, so that the effective interaction decays on the scale larger than in the two cases considered above.

It is remarkable that, similar to the NLS models with long-range dispersive interactions [27,28], we find a *non-monotonic* behavior of the mode power $Q(\omega)$ for this type of nonlinear photonic crystal waveguides: specifically, $Q(\omega)$ *increases* in the frequency interval $0.344 < (\omega a/2\pi c) < 0.347$ [shaded in Fig. 8(c)]. One can expect that, similar to the results earlier obtained for the nonlocal NLS models [27,28], the nonlinear localized modes in this interval are unstable and will eventually decay or transform into the modes of higher or lower frequency [29]. What counts is that there is an interval of mode power in which *two stable nonlinear localized modes of different widths do coexist*. Since the mode power is closely related to the mode energy, one can expect that the mode energy is also non-monotonic function of ω. Such a phenomenon is known as *bistability*, and in the problem under consideration it occurs as a direct manifestation of the nonlocality of the effective (linear and nonlinear) interaction between the defect rod sites.

Being interested in the mobility of the nonlinear localized modes we have investigated, in addition to the symmetric modes shown in the left inset in Fig. 7(b) and in Fig. 8(a), also the *antisymmetric localized modes* shown in Fig. 8(b). Our calculations show that the power $Q(\omega)$ of the antisymmetric modes always (for all values of ω and all types of waveguides) exceeds that for symmetric ones [see, e.g., Fig. 8(c)]. Thus, antisymmetric modes are expected to be unstable and they should transform into a lower-energy symmetric modes.

In fact, the difference between the power of antisymmetric and symmetric modes determines the Peierls-Nabarro barrier which should be overtaken for realizing the mobility of a nonlinear localized mode. One can see in Fig. 8(c) that the Peierls-Nabarro barrier is negligible for $0.347 < (\omega a/2\pi c) < 0.352$ and thus such localized modes should be mobile. However, the Peierls-Nabarro barrier becomes sufficiently large for highly localized modes with $\omega < 0.344 \times 2\pi c/a$ and, as a consequence, such modes should be immobile. Hence, the bistability phenomenon in the photonic crystal waveguides of the type depicted in Figs. 7–8 opens up fresh opportunities [28] for *switching* between immobile localized modes (used for the energy storage) and mobile localized modes (used for the energy transport).

The foregoing discussions on the mode mobility, based on the qualitative picture of the Peierls-Nabarro barrier, have been established for the discrete *one-dimensional* arrays. It is clear that the *two-dimensional* geometry of photonic crystals under consideration will bring new features into this picture. However, all these issues are still open and would require a further analysis.

6 Self-Trapping of Light in a Reduced-Symmetry 2D Nonlinear Photonic Crystal

A low-intensity light cannot propagate through a photonic crystal if the light frequency falls into a band gap. However, it has been recently suggested [13]

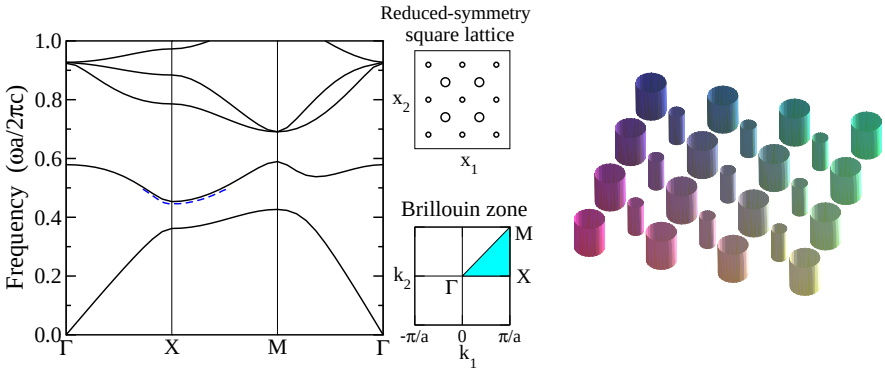

Fig. 9. Band-gap structure of the reduced-symmetry photonic crystal with $r_0 = 0.1a$, $r_d = 0.05a$, and $\varepsilon = 11.4$ for both types of rods. Full lines are calculated by the MIT Photonic-Bands program [31] whereas dashed line is found from the effective discrete model. The top center inset shows a cross-sectional view of the 2D photonic crystal depicted in the right inset. The bottom center inset shows the corresponding Brillouin zone.

that in the case of a 2D periodic medium with a Kerr-type nonlinear material, high-intensity light with frequency inside the gap can propagate in the form of *finite energy solitary waves – 2D gap solitons*. These solitary waves were found to be *stable* [13], but the conclusion was based on the coupled-mode equations valid for a *weak modulation* of the dielectric constant $\varepsilon(\boldsymbol{x})$. However, in real photonic crystals the modulation of $\varepsilon(\boldsymbol{x})$ is *comparable to its average value*. Thus, the results of Ref. [13] have a limited applicability to the properties of localized modes in *realistic photonic crystals*.

More specifically, the coupled-mode equations are valid if and only if the band gap Δ is vanishingly small, i. e. $\Delta \sim A^2$ where A is an effective amplitude of the mode, that is a small parameter in the multi-scale asymptotic expansions [32]. If we apply this model to describe nonlinear modes in a wider gap (see, e.g., discussions in Ref. [32]), we obtain a 2D nonlinear Schrödinger (NLS) equation known to possess *no stable localized solutions*. Moreover, the 2D localized modes described by the coupled-mode equations are expected to possess *an oscillatory instability* recently discovered for a broad class of coupled-mode Thirring-like equations [33]. Thus, it is clear that, if nonlinear localized modes do exist in realistic PBG materials, their stability should be associated with *different physical mechanisms* not accounted for by simplified continuum models.

In this Section we follow Ref. [17] and study the properties of nonlinear localized modes in a 2D photonic crystal composed of *two types of circular rods*: the rods of radius r_0 made from a linear dielectric material and placed at the corners of a square lattice with the lattice spacing a, and the rods of radius r_d made from a nonlinear dielectric material and placed at the center of each unit cell (see right inset in Fig. 9). Recently, such *photonic*

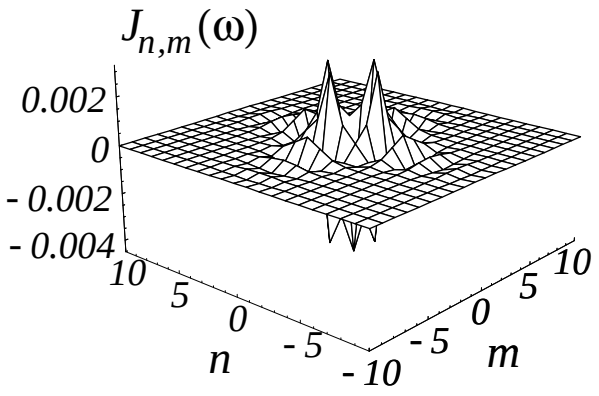

Fig. 10. Coupling coefficients $J_{n,m}(\omega)$ for the photonic crystal depicted in Fig. 9 (the contribution of the coefficient $J_{0,0} = 0.039$ is not shown). The frequency $\omega = 0.4456$ falls into the first band gap.

crystals of reduced symmetry have attracted considerable interest because of their ability to possess *larger absolute band gaps* [30]. The band-gap structure of the reduced-symmetry photonic crystal is shown in Fig. 9. As is seen, it possesses two band gaps, first of which extends from $\omega = 0.426 \times 2\pi c/a$ to $\omega = 0.453 \times 2\pi c/a$.

The reduced-symmetry "diatomic" photonic crystal shown in Fig. 9 can be considered as a square lattice of the "nonlinear defect rods" of small radius r_d ($r_d < r_0$) embedded into the ordinary single-rod photonic crystal formed by a square lattice of rods of larger radius r_0 in air. The positions of the defect rods can then be described by the vectors $\boldsymbol{x}_{n,m} = n\,\boldsymbol{a}_1 + m\,\boldsymbol{a}_2$, where $\boldsymbol{a}_1$ and $\boldsymbol{a}_2$ are the primitive lattice vectors of the 2D photonic crystal. Here, in contrast to the photonic crystal waveguides discussed in the previous section, the nonlinear defect rods are characterized by two integer indices, n and m. However, it is straightforward to extend Eq. (13) and write an approximate 2D discrete nonlinear equation

$$i\sigma\frac{\partial}{\partial t}E_{n,m} - E_{n,m} + \sum_{k,l} J_{n-k,\,m-l}(\omega)(\varepsilon_d^{(0)} + |E_{k,l}|^2)E_{k,l} = 0\,, \qquad (17)$$

for the amplitudes of the electric field $E_{n,m}(t\,|\,\omega) \equiv E(\boldsymbol{x}_{n,m}, t\,|\,\omega)$ inside the defect rods. We have checked the accuracy of the approximation provided by Eq. (17) solving it in the linear limit, in order to find the band-gap structure associated with linear stationary mode. Since the coupling coefficients $J_{n,m}(\omega)$ in the photonic crystal depicted in Fig. 9 are highly long-ranged functions (see Fig. 10), one should take into account the interaction between at least 10 neighbors to reach accurate results. As is seen from Fig. 9, in this

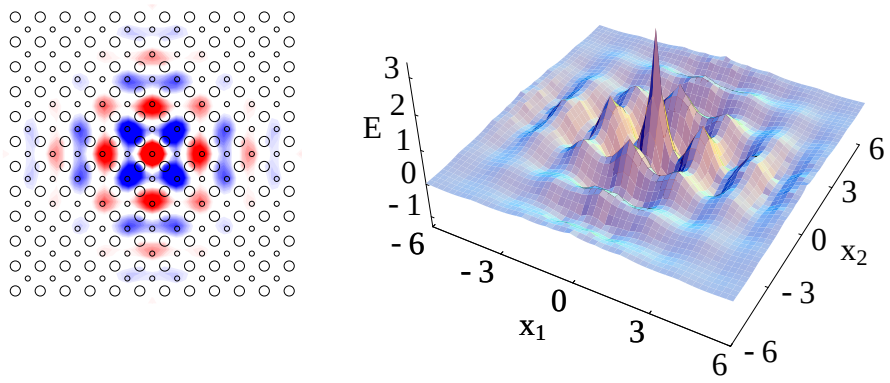

Fig. 11. Top (left) and 3D (right) views of a nonlinear localized mode in the first band gap of 2D photonic crystal depicted in Fig. 9.

case the frequencies of the linear modes (depicted by a dashed line, with a minimum at $\omega = 0.446 \times 2\pi c/a$) calculated from Eq. (17) are in a good agreement with those calculated directly from Eq. (2). It lends a support to the validity of Eq. (17) and allows us to use it for studying nonlinear properties.

Stationary nonlinear modes described by Eq. (17) are found numerically by the Newton-Raphson iteration scheme. We reveal the existence of *a continuous family of such modes*, and a typical example [smoothed by continuous optimization for Eq. (5)] of nonlinear localized mode is shown in Fig. 11. In Fig. 12, we plot the dependence of the mode power

$$Q(\omega) = \sum_{n,m} |E_{n,m}|^2 \,, \tag{18}$$

on the frequency ω for the photonic crystal shown in Fig. 9. As we have already discussed, this dependence represents a very important characteristic of nonlinear localized modes which allows to determine their stability by means of the Vakhitov-Kolokolov stability criterion: $dQ/d\omega > 0$ for unstable modes (this criterion has been extended [35] to 2D NLS models).

As is well known [35,36], in the 2D discrete cubic NLS equation, only high-amplitude localized modes are stable, whereas no stable modes exist in the continuum limit. For our model, the high-amplitude modes are also stable (see inset in Fig. 12), but they are not accessible under realistic conditions: To excite such modes one should increase the refractive index at the mode center in more than 2 times. Thus, for realistic conditions and relatively small values of $\chi^{(3)}$, only low-amplitude localized modes become a subject of much

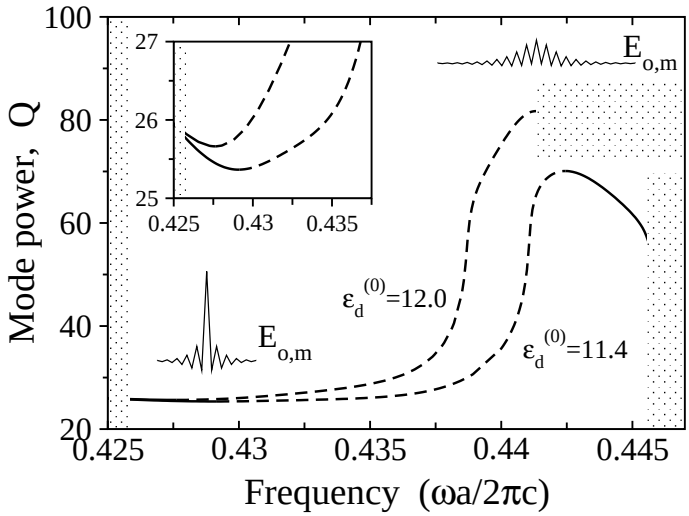

Fig. 12. Power Q vs. frequency ω for the 2D nonlinear localized modes in the photonic crystal of Fig. 9 with two different $\epsilon_d^{(0)}$. Solid lines – stable modes, dashed lines – unstable modes. Insets show typical profiles of stable modes, and an enlarged part of the power dependence. Grey areas show the lower and upper bands of delocalized modes surrounding the band gap.

interest since they can be excited in experiment. However, such modes in unbounded 2D NLS models are always unstable and either collapse or spread out [34]. In fact, they can be stabilized by some external forces (e.g., due to interactions with boundaries or disorder [37]), but in this case the excitations are pinned and cannot be used for energy or signal transfer.

Here we reveal that, in a sharp contrast to the 2D discrete NLS models discussed earlier in various applications, the low-amplitude localized modes of Eq. (17) can be stabilized due to *nonlinear long-range dispersion* inherent to the photonic crystals. It should be emphasized that such stabilization does not occur in the models with only *linear long-range* dispersion [34]. In order to gain a better insight into the stabilization mechanism, we have carried out the studies of Eq. (13) for the exponentially decaying coupling coefficients $J_{n,m}$. Our results show that the most important factor which determines stability of the low-amplitude localized modes is a ratio of the coefficients at the local nonlinearity ($\sim J_{0,0}$) and the nonlinear dispersion ($\sim J_{0,1}$). If the coupling coefficients $J_{n,m}$ decrease with the distances n and m rapidly, the low-amplitude modes of Eq. (17) with $\epsilon_d^{(0)} = 11.4$ are essentially stable for $J_{0,0}/J_{0,1} \leq 13$. However, this estimation is usually lowered because the stabilization is favored by the presence of long-range interactions.

It should be mentioned that the stabilization of low-amplitude 2D localized modes is not inherent to all types of nonlinear photonic crystals. On the contrary, the photonic crystals must be *carefully designed* to support *stable*

low-amplitude nonlinear modes. For example, in the photonic crystal considered above such modes are stable at least for $11 < \epsilon_d^{(0)} < 12$, however they become unstable for $\epsilon_d^{(0)} \geq 12$ (see Fig. 12). The stability of these modes can also be controlled by varying r_d, r_0, or ϵ_0.

7 Concluding Remarks

Exploration of nonlinear properties of PBG materials may open new important application of photonic crystals for all-optical signal processing and switching, allowing an effective way to create tunable band-gap structures operating entirely with light. Nonlinear photonic crystals, and nonlinear waveguides created in the photonic structures with a periodically modulated dielectric constant, create an ideal environment for the generation and observation of nonlinear localized modes.

As follows from our results, nonlinear localized modes can be excited in photonic crystal waveguides of different geometry. For several geometries of 2D waveguides, we have demonstrated that such modes are described by a new type of nonlinear lattice models that include long-range interaction and effectively nonlocal nonlinear response. It is expected that the general features of nonlinear guided modes described here will be preserved in other types of photonic crystal waveguides. Additionally, similar types of nonlinear localized modes are expected in photonic crystal fibers [38] consisting of a periodic air-hole lattice that runs along the length of the fiber, provided the fiber core is made of a highly nonlinear material (see, e.g., Ref. [39]).

Experimental observation of nonlinear photonic localized modes would require not only the use of photonic materials with a relatively large nonlinear refractive index (such as AlGaAs waveguide PBG structures [40] or polymer PBG crystals [41], but also a control of the group-velocity dispersion and band-gap parameters. The latter can be achieved by employing the surface coupling technique [42] that is able to provide coupling to specific points of the dispersion curve, opening up a very straightforward way to access nonlinear effects.

Acknowledgments

The authors are indebted to O. Bang, K. Busch, P.L. Christiansen, Yu.B. Gaididei, S. John, A. McGurn, C. Soukoulis, and A.A. Sukhorukov for encouraging discussions, and R.A. Sammut for collaboration at the initial stage of this project. The work has been partially supported by the Large Grant Scheme of the Australian Research Council and the Performance and Planning Foundation grant of the Institute of Advanced Studies.

References

1. J. D. Joannoupoulos, R. B. Meade, and J. N. Winn, *Photonic Crystals: Molding the Flow of Light* (Princeton University Press, Princeton N.J., 1995).
2. J. G. Fleming and S.-Y. Lin, Opt. Lett. **24**, 49 (1999).
3. See, e.g., K. Busch and S. John, Phys. Rev. Lett. **83**, 967 (1999), and discussions therein.
4. V. Berger, Phys. Rev. Lett. **81**, 4136 (1998); and also the recent experiment: N.G.R. Broderick, G.W. Ross, H.L. Offerhaus, D.J. Richardson, and D.C. Hanna, Phys. Rev. Lett. **84**, 4345 (2000); S. Saltiel and Yu.S. Kivshar, Opt. Lett. **25**, 1204 (2000).
5. See, e.g., S. Flach and C.R. Willis, Phys. Rep. **295**, 181 (1998); O.M. Braun and Yu.S. Kivshar, Phys. Rep. **306**, 1 (1998), Chap. 6.
6. R.S. MacKay and S. Aubry, Nonlinearity **7**, 1623 (1994); see also S. Aubry, Physica D **103**, 201 (1997).
7. B.I. Swanson, J.A. Brozik, S.P. Love, G.F. Strouse, A.P. Shreve, A.R. Bishop, W.Z. Wang, and M.I. Salkola, Phys. Rev. Lett. **82**, 3288 (1999).
8. U.T. Schwarz, L.Q. English, and A.J. Sievers, Phys. Rev. Lett. **83**, 223 (1999).
9. E. Trias, J.J. Mazo, and T.P. Orlando, Phys. Rev. Lett. **84**, 741 (2000); P. Binder, D. Abraimov, A.V. Ustinov, S. Flach, and Y. Zolotaryuk, Phys. Rev. Lett. **84**, 745 (2000).
10. F.M. Russel, Y. Zolotaryuk, and J.C. Eilbeck, Phys. Rev. B **55**, 6304 (1997).
11. H.S. Eisenberg, Y. Silberberg, R. Marandotti, A.R. Boyd, and J.S. Aitchison, Phys. Rev. Lett. **81**, 3383 (1998).
12. A.A. Sukhorukov, Yu.S. Kivshar, O. Bang, J. Martorell, J. Trull, and R. Vilaseca, Optics and Photonics News **10** (12) 34 (1999).
13. S. John and N. Aközbek, Phys. Rev. Lett. **71**, 1168 (1993); Phys. Rev. E **57**, 2287 (1998).
14. A.A. Sukhorukov, Yu.S. Kivshar, and O. Bang, Phys. Rev. E **60**, R41 (1999).
15. A. R. McGurn, Phys. Lett. A **251**, 322 (1999); Phys. Lett. A **260**, 314 (1999).
16. S. F. Mingaleev, Yu. S. Kivshar, and R. A. Sammut, Phys. Rev. E **62**, 5777 (2000).
17. S. F. Mingaleev and Yu. S. Kivshar, Phys. Rev. Lett. **86** (June 2001), in print [arXiv:cond-mat/0102066].
18. A. A. Maradudin and A. R. McGurn, in *Photonic Band Gaps and Localization*, *NATO ASI Series B: Physics*, Vol. 308, Ed. C. M. Soukoulis (Plenum Press, New York, 1993), p. 247.
19. A. Mekis, J.C. Chen, I. Kurland, S. Fan, P.R. Villeneuve, and J.D. Joannopoulos, Phys. Rev. Lett. **77**, 3787 (1996).
20. A. Mekis, S. Fan, and J. D. Joannopoulos, Phys. Rev. B **58**, 4809 (1998).
21. A. J. Ward and J. B. Pendry, Phys. Rev. B **58**, 7252 (1998).
22. S.-Y. Lin, E. Chow, V. Hietala, P.R. Villeneuve, and J.D. Joannopoulos, Science **282**, 274 (1998).
23. M. Tokushima, H. Kosaka, A. Tomita, and H. Yamada, Appl. Phys. Lett. **76**, 952 (2000).
24. S. S. M. Cheng, L. M. Li, C. T. Chan, and Z. Q. Zhang, Phys. Rev. B **59**, 4091 (1999).
25. C. Jin, B. Cheng, B. Mau, Z. Li, D. Zhnag, S. Ban, B. Sun, Appl. Phys. Lett. **75**, 1848 (1999).

26. S. Fan, P. R. Villeneuve, J. D. Joannopoulos, and H. A. Haus, Phys. Rev. Lett. **80**, 960 (1998).
27. Y. B. Gaididei, S. F. Mingaleev, P. L. Christiansen, and K. Ø. Rasmussen, Phys. Rev. E **55**, 6141 (1997).
28. M. Johansson, Y. B. Gaididei, P. L. Christiansen, and K. Ø. Rasmussen, Phys. Rev. E **57**, 4739 (1998).
29. See, e.g., the examples for the continuous generalised NLS models, D. E. Pelinovsky, V. V. Afanasjev, and Yu. S. Kivshar, Phys. Rev. E **53**, 1940 (1996).
30. C. M. Anderson and K. P. Giapis, Phys. Rev. Lett. **77**, 2949 (1996); Phys. Rev. B **56**, 7313 (1997).
31. S. G. Johnson, http://ab-initio.mit.edu/mpb/
32. Yu. S. Kivshar, O. A. Chubykalo, O. V. Usatenko, and D. V. Grinyoff, Int. J. Mod. Phys. B **9**, 2963 (1995).
33. I. V. Barashenkov, D. E. Pelinovsky, and E. V. Zemlyanaya, Phys. Rev. Lett. **80**, 5117 (1998); A. De Rossi, C. Conti, and S. Trillo, Phys. Rev. Lett. **81**, 85 (1998).
34. See, e.g., V. K. Mezentsev, S. L. Musher, I. V. Ryzhenkova, and S. K. Turitsyn, JETP Lett. **60**, 829 (1994); S. Flach, K. Kladko, and R. S. MacKay, Phys. Rev. Lett. **78**, 1207 (1997); P. L. Christiansen *et al.*, Phys. Rev. B **57**, 11303 (1998).
35. E. W. Laedke *et al.*, JETP Lett. **62**, 677 (1995).
36. E. W. Laedke, K. H. Spatschek, S. K. Turitsyn, and V. K. Mezentsev, Phys. Rev. E **52**, 5549 (1995); Yu. B. Gaididei, P. L. Christiansen, K. Ø. Rasmussen, and M. Johansson, Phys. Rev. B **55**, R13365 (1997).
37. Yu. B. Gaididei, D. Hendriksen, P. L. Christiansen, and K. Ø. Rasmussen, Phys. Rev. B **58**, 3075 (1998).
38. T.A. Birks, J.C. Knight, and P.St.J. Russell, Opt. Lett. **22**, 961 (1997).
39. B.J. Eggleton, P.S. Westbrook, R.S. Windeler, S. Spälter, and T.A. Strasser, Opt. Lett. **24**, 1460 (1999).
40. P. Millar *et al.*, Opt. Lett. **24**, 685 (1999); A.A. Helmy *et al.*, Opt. Lett. **25**, 1370 (2000).
41. S. Shoji and S. Kawata, Appl. Phys. Lett. **76**, 2668 (2000).
42. V. N. Astratov *et al.*, Phys. Rev. B **60**, R16255 (1999).